# Interferometric coherent Fourier scatterometry: a method for obtaining high sensitivity in the optical inverse-grating problem

Roy, S; Kumar, N; Pereira, SF; Urbach, HP

**DOI**
10.1088/2040-8978/15/7/075707

**Publication date**
2013

**Document Version**
Final published version

**Published in**
Journal of Optics

# Interferometric coherent Fourier scatterometry: a method for obtaining high sensitivity in the optical inverse-grating problem

IOP Publishing Journal of Optics
J. Opt. **15** (2013) 075707 (9pp) doi:10.1088/2040-8978/15/7/075707

# Interferometric coherent Fourier scatterometry: a method for obtaining high sensitivity in the optical inverse-grating problem

**S Roy, N Kumar, S F Pereira and H P Urbach**

Optics Research Group, Delft University of Technology, PO Box 5046, 2600 GA Delft, The Netherlands

E-mail: S.Roy@tudelft.nl

Received 25 January 2013, accepted for publication 8 May 2013
Published 4 June 2013
Online at stacks.iop.org/JOpt/15/075707

**Abstract**
In recent times, coherent Fourier scatterometry has been considered as an emerging optical grating scatterometry technique for semiconductor metrology since it shows large sensitivity owing to its scanning ability. However, further utilization of coherence is possible by making additional measurements using the principle of temporal phase-shifting interferometry. In this paper, through numerical simulation, we show how scanning and interferometry can be coupled together to improve the sensitivity of coherent Fourier scatterometry, to extend its range of applicability and to obtain sufficient information to calculate the complex scattering matrix for all angles of incidences inside the numerical aperture of a microscope objective.

**Keywords:** scatterometry, grating, lithography inspection, coherence, interferometry

(Some figures may appear in colour only in the online journal)

## 1. Introduction

With the advancement of semiconductor technology, not surprisingly, a rapid increase in nano-metrology tools suitable for industrial uses is being observed. However, a look at the recent ITRS roadmap [1] reveals that there are still many cases where the required accuracies are not met by tools that exist at present. Industrial nano-metrology techniques must be fast, non-contact and process integrable without loss of accuracy. Optical inverse-grating scatterometry, in which the shape of a grating sample is retrieved from far field measurements followed by numerical optimization, is one of the few methods fulfilling all these requirements [2]. Owing to its practical importance, a number of articles have been devoted to scatterometry, so that a detailed introduction can be skipped here, while [3] or [4] can be referred to for a review.

The state of the art optical scatterometry technique that is presently used in industry is incoherent Fourier scatterometry, in which a spatially incoherent extended light source and Köhler illumination are used [5]. Every source point corresponds to a particular plane wave that is incident on the grating. Because the light source is spatially incoherent, the incident plane waves are mutually incoherent. The intensities of the scattered orders that are captured by the lens are measured and compared to simulations, from which the grating parameters are determined. Gawhary *et al* [6] introduced coherent Fourier scatterometry (CFS), in which a coherent source and a high NA focusing lens are applied to illuminate the grating with a focused spot. The focused spot can be expanded in mutually coherent plane waves that are incident on the grating. The intensities of the reflected orders that are captured by the objective are measured and compared to simulations. By using two polarizers, one in the incident beam and the other in the reflected beam (after collimation by the lens), all combinations of incident and reflected polarizations are measured. If the pitch and the numerical aperture of the objective are so large that higher reflected orders are captured by the lens, then some of the

 

reflected orders overlap. This happens in both incoherent and coherent Fourier scatterometry, but since in incoherent Fourier scatterometry the contributing orders are mutually incoherent, the total intensity is the sum of the intensities of the overlapping orders. In contrast, in CFS the overlapping orders interfere and the measured total intensity depends on the phase difference between them. As has been shown in [7], the intensities and phase differences of the overlapping orders can be retrieved by scanning the focused spot over a period of the grating. Since the method is similar to a common path interferometer, it is robust. The information about the overlapping orders can be retrieved in CFS provided the pitch is large enough. Since this is lacking in incoherent Fourier scatterometry, the sensitivity for grating shape parameters is considerably higher in CFS [8]. If the pitch is so small that reflected orders higher than the zeroth order cannot be captured by the lens, there is no difference in sensitivity between the coherent and incoherent versions of Fourier scatterometry.

However, in CFS, information about the phase differences between different scattered waves is available only, not about their individual phases. If this information were also available an even higher sensitivity could be expected. The only conceivable way to retrieve this phase information is by letting the reflected spot interfere with a reference beam [9]. We shall refer to the combination of CFS with interferometry as interferometric coherent Fourier scatterometry (ICFS). With this motivation, the purpose of this paper is to investigate by simulations the gain in sensitivity that can be expected with these combined techniques. The intensities and phase differences of overlapping orders are again obtained by scanning the spot, just as in conventional CFS, whereas the phase of the total scattered field is obtained by interfering the reflected spot with a reference beam. The latter can always be carried out whatever the value of the pitch; hence, in contrast to CFS, ICFS always gives a higher sensitivity compared to incoherent Fourier scatterometry, even for a very small pitch. Two orthogonal polarizations are again chosen for the incident field and in each case the polarization of the reference beam is chosen parallel to that of the incident field. As will be shown in this paper, with ICFS the complete complex scattering matrices can be determined for all reflected orders and all incident waves inside the numerical aperture of the lens. Hence, for a given NA, with ICFS the maximum possible information about the scattered far field (i.e., the intensities and phases for all combinations of incident and reflected polarization states) is used to reconstruct the grating parameters. Interestingly, we will show that by adding interferometry, the minimum number of scanning positions that is needed to retrieve the overlapping orders is *less* than in conventional CFS. Recently, an extension of CFS with white light interferometry has been reported [10], where a polychromatic source has been used to produce a reference wave that interferes with the scattered wave from the sample. Essentially, this technique utilizes the advantages of spectroscopic scatterometry in a modified CFS setup. Besides experimental complexity, the main drawback with spectroscopic scatterometry for semiconductor industries is unwanted exposure of photo-resist by short wavelength components. Thus, angular scatterometry with larger wavelengths is preferred. However, interference with a monochromatic source should lead us closer to determining the full scattering matrix [11] of the system, and so towards maximum sensitivity to solve the ill-posed [12] inverse-grating problem. Also, it should allow us to limit the size of the data, thereby helping to achieve faster optimization.

Goniometric scatterometry [13, 14] is probably the most well known angular scatterometry technique. As illustrated in figure 1(a), plane waves corresponding to a certain set of incident angles interact with the grating one by one and the intensities of the reflected orders are measured for all combinations of orthogonal states of the polarizers in the incident and scattered beams. Since the grating is illuminated by one plane wave at a time, goniometric scatterometry is too slow for most applications. Nevertheless, if this technique is extended by interferometry with a reference beam, the full information about the complex scattering matrix can be retrieved, just as in ICFS. One might thus expect that the sensitivity for the grating parameters of interferometric goniometric scatterometry must be the same as for ICFS. However, as we will explain, in fact the sensitivity of ICFS is larger if the pitch of the grating is large. Hence, ICFS is not only a very fast alternative for interferometric goniometric scatterometry but also has superior sensitivity.

This paper is organized as follows. In section 2 we describe the model for CFS and ICFS. In section 3 we present the results of simulations and we discuss the improvement that is obtained with ICFS. The final section, section 4, contains the conclusions.

## 2. Modeling of the coherent Fourier scatterometry

The problem of the interaction of a plane wave and a periodic structure is well studied and needs little introduction. We introduce a Cartesian coordinate system $(x, y, z)$ as shown in figure 1, such that the grating is periodic in the $x$-direction, the grooves are parallel to the $y$-axis and the $z$-axis is the optical axis of the focusing system such that $z$ increases in the direction of propagation of the incident beam with $z = 0$ coinciding with the top of the grating.

The incident spot can be expanded into plane waves that are incident on the grating. The sine of the angle of incidence of these plane waves with the $z$ axis is smaller than the numerical aperture (NA) of the focusing lens. The interaction of an incident plane wave with the grating leads to diffracted orders. The propagating reflected orders, for which the sine of the angle with the normal of the grating is smaller than the NA, are captured by the lens and detected by a camera conjugate with the lens pupil. Every plane wave whose angle of incidence or angle of reflection with the normal of the grating is within the numerical aperture (NA) of the lens corresponds to a point in the pupil of the lens. Depending on the value of the so-called overlap parameter introduced in [6],

$$F = \frac{\lambda}{\Lambda\ \mathrm{NA}}, \tag{1}$$

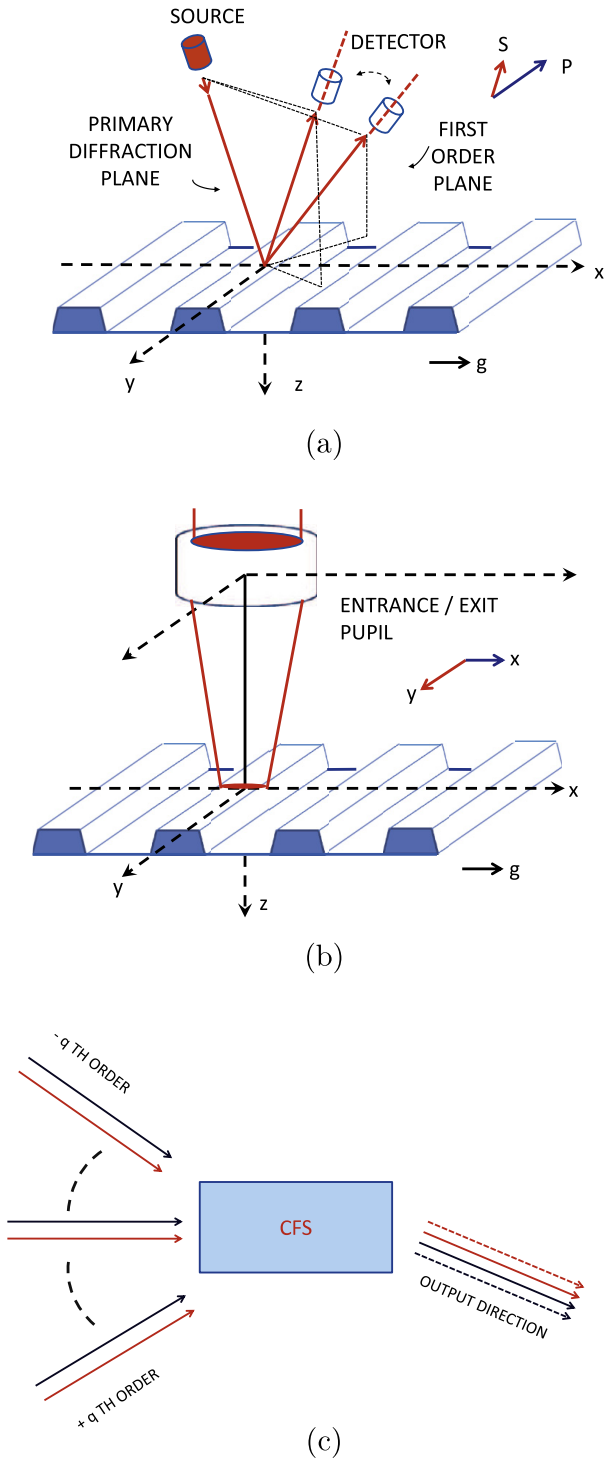


**Figure 1.** The schematics of coherent goniometric scatterometry and CFS for a one-dimensional grating. The coordinate system $(x, y, z)$ is such that $x$ is the direction of periodicity, $y$ is the direction of translational invariance of the grating and $z$ coincides with the optical axis of the objective. Thus, the grating vector $\mathbf{g}$ has only an $x$-component. Two different orthogonal polarizations are shown in different colors, red and blue. In (a) and (b), respectively, simple schematics of coherent goniometric scatterometry and CFS systems are shown. In (c) a block diagram of a CFS system is illustrated. Here, we look at one outgoing direction in the pupil plane in which several incident 'red' or 'blue' waves can contribute depending on the pitch of the grating. When practically realized, (red, blue) can be seen as (S, P) in coherent goniometric scatterometry and $(y, x)$ in CFS.

where $\Lambda$ is the pitch of the grating and $\lambda$ is the illumination wavelength, a certain number $N$ of reflected orders can overlap. If $1 < F \leq 2$, then the $+1$st, $-1$st and 0th order are captured by the lens. Consequently, for some directions of the reflected beam, the total complex amplitude is the sum of a field that is the 0th reflected order of some incident beam and a field that is the $+1$st reflected order of another incident beam. As long as $F > 1$, the $-1$st and $+1$st reflected orders never overlap, hence for $1 < F \leq 2$ we have $N = 2$. As an example of the superposition for $N = 2$, in figure 2(a) the contributing orders are the zeroth from $Q_0$ and the first from $Q_1$, which appear at the pupil point $Q$ corresponding to the scattered wavevector $\mathbf{k}^s_Q$. The adjacent figure 2(b) explains how the focusing by the objective is modeled.

In incoherent Fourier scatterometry, the overlapping orders are mutually incoherent, hence the total intensity is the sum of the intensities of the orders, but in CFS they are coherent and hence interfere. If there is no way to separate the waves, then the information content in the measurements is not properly utilized, and the sensitivity of CFS is not optimal. For this reason, scanning of the sample after illumination by coherent light is to be utilized. Figure 3(a) shows the scanning scheme for a one-dimensional grating, with the grating vector along $x$, as the grating is moved along $x$ through small uniform steps until the whole pitch is covered. The number of steps, or number of sufficient scanning positions ($\beta_{\min}$), depends on whether there is superposition between the orders or not. Thus, it is related directly to $F$. If $F > 2$, there is no overlap of the reflected orders (only the 0th reflected order is detected), making scanning unnecessary. The scanning becomes necessary when the superposition of orders starts at $F \leq 2$ (as the first order starts to be captured by the optical system ($N > 1$)). The second order is captured if $0.67 < F \leq 1$. As the number of superposing orders is determined solely by $F$, the minimum number of scanning positions ($\beta_{\min}$) needed to obtain maximum sensitivity can be determined directly from $F$ [7, 8][1].

To simulate CFS for an objective of given NA, it is convenient to define an orthonormal basis $(\hat{\boldsymbol{\xi}}, \hat{\boldsymbol{\eta}})$ in the lens pupil which is parallel to the $(\hat{\mathbf{x}}, \hat{\mathbf{y}})$-basis. The incident field at a given point $Q$ of the pupil having pupil coordinates $(\xi, \eta)$ is related to a unique plane wave incident on the grating with a wavevector whose projection on the $(x, y)$-plane is given by (see figure 2(b))

$$\mathbf{k}^i_Q = -nk_0(\xi\hat{\mathbf{x}} + \eta\hat{\mathbf{y}}), \tag{2}$$

where $n$ is the refractive index of the ambient medium, $k_0$ is the vacuum wavenumber and $\mathbf{k}^i_Q$ is the incident wavevector. In this paper we will be using superscript $s$ for scattered wave and superscript $i$ for incident wave. Since the $z$-component of the

[1] For CFS, $\beta_{\min} = 1$ if $F > 2$, $\beta_{\min} = 4$ in the range $1 < F \leq 2$, $\beta_{\min} = 6$ in the range $0.67 < F \leq 1$ etc. It should be noted that $\beta_{\min} = 3$ would have been sufficient when $1 < F \leq 2$, but for simplicity in modeling it is convenient to choose scan positions symmetrically about the center of the pitch. Also, it is convenient to assume that in the initial position without scan, the optical axis ($z$-axis) passes through the center of the pitch, as shown in figure 3(a). In the experimental situation this is not possible, and the misalignment is introduced as an additional parameter to be reconstructed. For details, refer to [8].

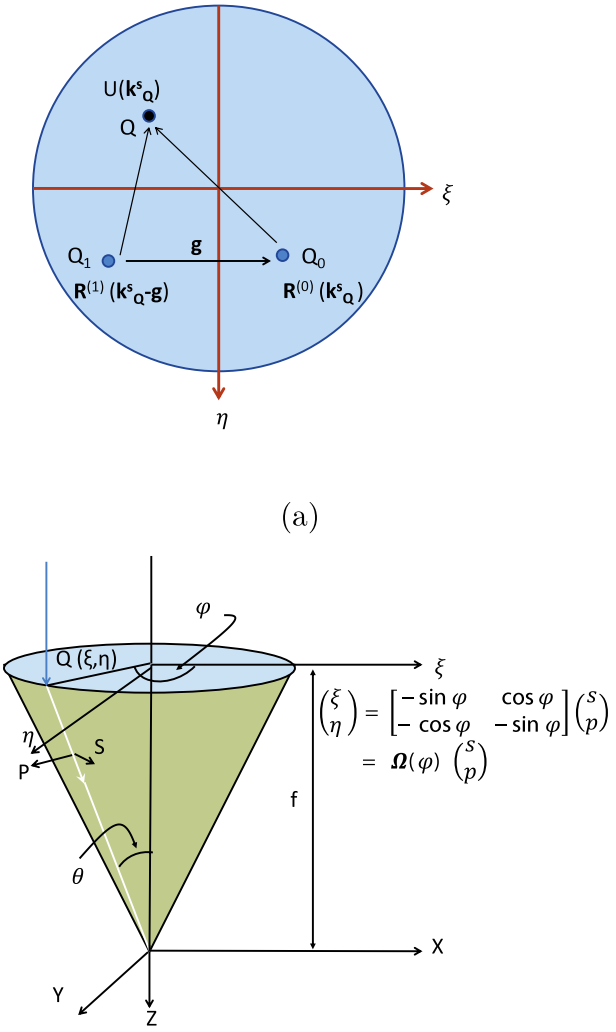


**Figure 2.** (a) The objective pupil plane where a point $Q$, which corresponds to the scattered transverse wavevector $\mathbf{k}^{\mathrm{s}}_Q$, is contributed by the waves from direction $\mathbf{k}^{\mathrm{s}}_Q$ (corresponding to point $Q_0$) and $\mathbf{k}^{\mathrm{s}}_Q - \mathbf{g}$ (corresponding to point $Q_1$), respectively, through the superposition of their zeroth and first orders. Here, $\mathbf{g}$ is the grating vector and $\hat{\boldsymbol{\xi}}$, $\hat{\boldsymbol{\eta}}$ is the orthonormal basis at the pupil plane parallel to the $(\hat{\mathbf{x}}, \hat{\mathbf{y}})$-basis, with $-\mathrm{NA} \le \xi, \eta \le \mathrm{NA}$. (b) An illustration of how the focusing action of the objective is modeled. The objective transforms a ray incident at $Q(\xi, \eta)$ on its pupil plane to a plane wave of incidence angle $(\theta, \varphi)$. They are related by $\varphi = \tan^{-1}(\eta/\xi)$ and $\theta = \sin^{-1}\sqrt{\xi^2 + \eta^2}$. The polarization of the incident ray is set to be in the pupil plane by a polarizer placed before the objective (not shown here) and, thus, expressible in $\hat{\boldsymbol{\xi}}$, $\hat{\boldsymbol{\eta}}$. It is also required to transform this polarization from basis $\hat{\boldsymbol{\xi}}$, $\hat{\boldsymbol{\eta}}$ to S, P relative to the plane of incidence. This is carried out in two steps: first the rotation matrix $\boldsymbol{\Omega}(\varphi)$ is used to transform from $\hat{\boldsymbol{\xi}}$, $\hat{\boldsymbol{\eta}}$ to an intermediate polar basis, and then this is transformed into the S, P basis with a unit matrix. Given the S, P components and the angles $\theta$, $\varphi$, one has sufficient information to define the incident wave on the grating.

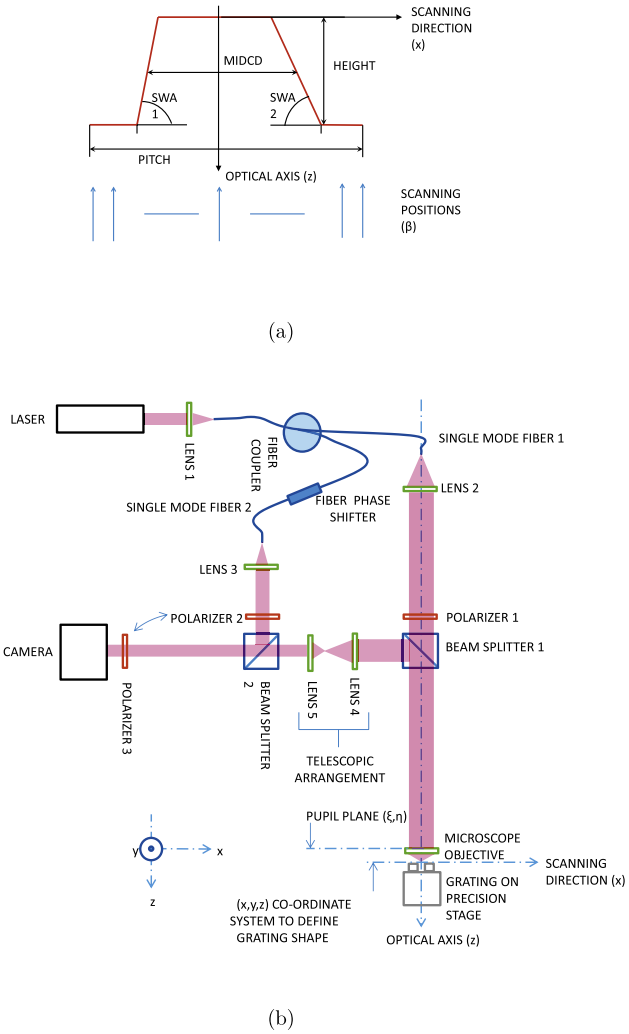


**Figure 3.** The grating parameters and the scanning are defined in (a). In the modeling, the center of the pitch is assumed to be on the $z$-axis without scan (initial position). The scanning positions are designated by $\beta$, with $\beta = (0, 1, \ldots, \beta_{\min} - 1)$. If the grating vector has only an $x$-component, scanning is needed only along $x$ and the $\beta$th scanning position denotes a shift of $\beta\Delta x$ from the origin ($\Delta x$ is the scanning step size). (b) A possible scheme of the interferometric coherent scatterometry setup. The coordinate plane $x$–$y$ is located in the back focal plane of the objective. The fiber coupler creates the reference and incident waves from an intensity stabilized laser. The scattered wave from the sample and the reference are superposed on beam splitter 2. Polarizers 2 and 3 are always parallel, as indicated by the arrow. The scanning is performed by a precision stage on which the sample is placed, whereas the reference phase shifts are introduced by a fiber phase shifter. Polarizer 1 sets the polarization of the incident wave.

wavevector is fixed once $\mathbf{k}^{\mathrm{i}}_Q$ is specified, $\mathbf{k}^{\mathrm{i}}_Q$ can be thought of as a unique direction. Each wavevector $\mathbf{k}^{\mathrm{s}}_Q$ of the field scattered by the grating is similarly related to a particular pupil point similarly as equation (2). For example, in figure 2(a), for $Q, \xi, \eta < 0$ and for $Q_0, \xi, \eta > 0$, etc.

Now suppose that reflected orders $m$ with $-M_1 < m < M_2$ contribute to the reflected wave with transverse wavevector $\mathbf{k}^{\mathrm{s}}_Q$ corresponding to pupil point $Q$. Here, $M_1$ and $M_2$ are the maximum numbers of negative and positive orders, respectively, which can be captured by the optical system and contribute to the total field of this reflected wave, (i.e., we have $N = M_1 + M_2 + 1$, with $N$ as introduced earlier). According to

Floquet's theorem, the transverse components of the incident wavevector $\mathbf{k}^{\mathrm{i}}_{m,Q}$ whose $m$th reflected order is in the direction of $\mathbf{k}^{\mathrm{s}}_{Q}$ satisfy

$$\mathbf{k}^{\mathrm{s}}_{Q} = \mathbf{k}^{\mathrm{i}}_{m,Q} + m\mathbf{g}. \tag{3}$$

Here, we must keep in mind that when expressed in terms of $\xi$ and $\eta$, the scattered and incident wavevectors will have components with opposite signs, in accordance with the laws of vector addition. Also, as illustrated in figure 2, $\mathbf{g}$ is the grating vector, which for our one-dimensional grating is given by (figure 1)

$$\mathbf{g} = \frac{2\pi}{\Lambda}\hat{\boldsymbol{\xi}}. \tag{4}$$

With this, we can write the total complex reflected field $\mathbf{b}$ at the pupil point $Q$ as

$$\mathbf{b}(\mathbf{k}^{\mathrm{s}}_{Q}) = \sum_{m=-M_1(\mathbf{k}^{\mathrm{i}}_{m,Q})}^{M_2(\mathbf{k}^{\mathrm{i}}_{m,Q})} \mathbf{R}_m(\mathbf{k}^{\mathrm{i}}_{m,Q})\mathbf{a}(\mathbf{k}^{\mathrm{i}}_{m,Q}). \tag{5}$$

Here, $\mathbf{R}_m(\mathbf{k}^{\mathrm{i}}_{m,Q})$ is the $2\times2$ matrix giving $m$th order complex diffraction amplitudes in reflection, for a wave with complex amplitude $\mathbf{a}(\mathbf{k}^{\mathrm{i}}_{m,Q})$ incident from the direction with transverse projection $\mathbf{k}^{\mathrm{i}}_{m,Q}$. Note that the reflection matrix in (5) relates fields in the lens pupil, i.e. $\mathbf{b}$ and $\mathbf{a}$ are both fields in the pupil. The reason for this is that the polarizer of the incident field is in the entrance pupil of the lens before focusing and the analyzer of the reflected beam is in the exit pupil after collimation. The incident field $\mathbf{a}$ in the pupil can be measured (amplitude and phase) by a wavefront sensor and can be expressed as a complex vector field dependent on the pupil coordinates $(\xi, \eta)$. Given the incident wavevector $\mathbf{k}^{\mathrm{i}}_{m,Q}$, the matrix $\mathbf{R}_m$ is dependent on the shape of the grating, and so is of central interest to us. In the basis $\hat{\boldsymbol{\xi}}, \hat{\boldsymbol{\eta}}$ we write the reflection matrix as

$$\mathbf{R}_{m;\,\Delta x}(\mathbf{k}^{\mathrm{i}}_{m,Q}) = \begin{pmatrix} r_m^{\xi\xi}(\mathbf{k}^{\mathrm{i}}_{m,Q}) & r_m^{\xi\eta}(\mathbf{k}^{\mathrm{i}}_{m,Q}) \\ r_m^{\eta\xi}(\mathbf{k}^{\mathrm{i}}_{m,Q}) & r_m^{\eta\eta}(\mathbf{k}^{\mathrm{i}}_{m,Q}) \end{pmatrix}, \tag{6}$$

where, for example, superscript $\xi\eta$ denotes polarization scheme $\xi$ in the reflected field and $\eta$ in the incident field (figure 2(b)), etc. The overall phase factor, which forms the basis of scanning, appears due to shift of the grating by $\Delta x$ (measured from the $z$-axis to the center of the pitch when the grating is in a specific scanning position) along the $x$-axis.

A general conically incident incoming wave with azimuthal angle $\varphi$ and incidence angle $\theta$ can be split into S and P polarized components (with respect to the plane of incidence), rigorously solved for an interaction with the grating, and the output field can be similarly expanded. The commonly used reflection matrix for the interaction of a plane wave with a grating gives the reflection coefficients of the reflected orders with respect to this basis. To distinguish it from the matrix defined above, we will denote this matrix for order $m$ by $\mathbf{R}^R_m$. Its relation with $\mathbf{R}_{m,\Delta x}$ is (see [7] for details)

$$\mathbf{R}_{m,\Delta x} = f(\theta,\theta_m)\boldsymbol{\Omega}(\varphi)\mathbf{R}^R_m\boldsymbol{\Omega}^{-1}(\varphi_m)\exp(\mathrm{j}mg\Delta x). \tag{7}$$

Here, $\Omega(\varphi_m)^{-1}$ is a rotation matrix that relates the incident field in pupil point $Q_m$ with polar coordinates $(\rho_m, \varphi_m)$ of the lens from the $\hat{\boldsymbol{\xi}}, \hat{\boldsymbol{\eta}}$ basis to the S, P basis. This intermediate basis $(\rho, \varphi)$ is essentially illustrated in figure 2(b). Pupil point $Q_m$ corresponds to the incident wavevector $\mathbf{k}^{\mathrm{i}}_{m,Q}$ whose $m$th reflected order is in the direction of the reflected wavevector $\mathbf{k}^{\mathrm{s}}_{Q}$ which, in turn, corresponds to pupil point $Q$ with coordinates $(\rho, \varphi)$. The reflection matrix $\mathbf{R}^R_m$ gives the reflected $m$th order in the S- and P-basis. The rotation matrix $\Omega(\varphi)$ transfers the S- and P-components of the $m$th reflected order with wavevector $\mathbf{k}^{\mathrm{s}}_{Q}$ back to the basis $\hat{\boldsymbol{\xi}}, \hat{\boldsymbol{\eta}}$ in the pupil point $Q$ (see figure 2(b)). Thus, $\mathbf{R}_{m,\Delta x}$ can be assumed to operate on the basis $\hat{\boldsymbol{\xi}}, \hat{\boldsymbol{\eta}}$ only. The scalar factor $f(\theta, \theta_m)$ is necessary for conservation of the energy flux[2].

Going back to equation (6), for each direction of scattering, the whole reflection process can be expressed by a set of $N$ complex $2 \times 2$ matrices. Our main interest in this paper is to obtain sufficient information to determine these scattering matrices. Let us assume for simplicity that in an experiment with the $\mu$–$\nu$ polarization scheme ($\mu$ or $\nu$ can each be either $\xi$ or $\eta$) only the zeroth and the first orders are captured and superposed, i.e., $1 < F \leq 2$. This is the case shown in figure 2(a). The complex amplitude of the reflected wave in the direction of $\mathbf{k}^{\mathrm{s}}_{Q}$ is then given by

$$b^{\mu\nu}_{\Delta x}(\mathbf{k}^{\mathrm{s}}_{Q}) = r_0^{\mu\nu}(\mathbf{k}^{\mathrm{s}}_{Q})a^{\nu}(\mathbf{k}^{\mathrm{s}}_{Q}) + r_1^{\mu\nu}(\mathbf{k}^{\mathrm{s}}_{Q} - \mathbf{g})a^{\nu}(\mathbf{k}^{\mathrm{s}}_{Q} - \mathbf{g}) \times \exp(\mathrm{j}mg\Delta x), \tag{8}$$

where equation (3) has been used to express the incident wavevectors in terms of the scattered wavevector. By symmetry, a similar expression will hold for superposition of the zeroth and the negative first orders, but the positive and negative first orders do not superpose unless $F < 1$. Thus, we can consider only one of the superpositions, namely, equation (8), and the analysis for the other one will be identical. The intensity in the pupil plane is

$$\begin{aligned} |b^{\mu\nu}_{\Delta x}(\mathbf{k}^{\mathrm{s}}_{Q})|^2 = {} & |r_0^{\mu\nu}(\mathbf{k}^{\mathrm{s}}_{Q})a^{\nu}(\mathbf{k}^{\mathrm{s}}_{Q})|^2 + |r_1^{\mu\nu} \\ & \times (\mathbf{k}^{\mathrm{s}}_{Q} - \mathbf{g})a^{\nu}(\mathbf{k}^{\mathrm{s}}_{Q} - \mathbf{g})|^2 \\ & + 2|r_0^{\mu\nu}(\mathbf{k}^{\mathrm{s}}_{Q})a^{\nu}(\mathbf{k}^{\mathrm{s}}_{Q})||r_1^{\mu\nu} \\ & \times (\mathbf{k}^{\mathrm{s}}_{Q} - \mathbf{g})a^{\nu}(\mathbf{k}^{\mathrm{s}}_{Q} - \mathbf{g})| \\ & \times \cos[(\arg r_0^{\mu\nu}(\mathbf{k}^{\mathrm{s}}_{Q}) - \arg r_1^{\mu\nu}(\mathbf{k}^{\mathrm{s}}_{Q} - \mathbf{g}) \\ & + \arg a^{\nu}(\mathbf{k}^{\mathrm{s}}_{Q}) - \arg a^{\nu}(\mathbf{k}^{\mathrm{s}}_{Q} - \mathbf{g}) - g\Delta x)], \end{aligned} \tag{9}$$

where $\arg(r_m^{\mu\nu})$ and $\arg(a^{\nu})$ are, respectively, the phases of the diffraction amplitudes and of the $\nu$th component of the incident field. The latter can be kept as a reference to be used if explicit phase evaluation from equation (8) is required. Thus, if we assume that the incident field is faithfully measured so that the vector $\mathbf{a}$ is known for all wavevector projections in the pupil, then (9) can be regarded as an equation with three unknowns, namely the moduli $|r_0^{\mu\nu}(\mathbf{k}^{\mathrm{s}}_{Q})|$ and $|r_1^{\mu\nu}(\mathbf{k}^{\mathrm{s}}_{Q} - \mathbf{g})|$ and the phase difference $\arg r_0^{\mu\nu}(\mathbf{k}^{\mathrm{s}}_{Q}) - \arg r_1^{\mu\nu}(\mathbf{k}^{\mathrm{s}}_{Q} - \mathbf{g})$. Following the standard algorithms of phase-shifting interferometry, we

[2] This is the ratio of square roots of cosines of incidence and scattered angles.

require at least three scanning positions to obtain all the unknowns in equation (9). This can be carried out by changing $\Delta x$ and repeating the measurements. This argument can be extended when more orders overlap, by stating that we need at least $2N-1$ scan positions for $N$ overlapping orders. Anyway, only the phase *difference* between overlapping reflected orders, i.e. $\arg r_0^{\mu\nu}(\mathbf{k}_Q^s) - \arg r_1^{\mu\nu}(\mathbf{k}_Q^s - \mathbf{g})$, can be calculated. This shows why scanning is not sufficient for determining the individual phases of the orders, and to obtain these, interference with a reference wave is necessary. This will be accompanied by an increase in the amount of data. This combined technique, which we introduce here as ICFS, will contain $4L\beta_{\min}\alpha_{\min}$ data elements, where $\alpha_{\min}$ is the required number of steps of phase-shifting interferometry and $\beta_{\min}$ is the minimum number of scanning positions (which may be different from $\beta_{\min}$ of CFS). Both of these are determined in the following equations.

If the reflected field $b_{\Delta x}^{\mu\nu}$ is made to interfere with another completely known reference wave $a_{\text{ref}}$ polarized along $\mu$, the output polarization direction, the complex amplitude becomes

$$a_{\text{ref}}^{\mu} + b_{\Delta x}^{\mu\nu}(\mathbf{k}_Q^s) = r_0^{\mu\nu}(\mathbf{k}_Q^s)a^{\nu}(\mathbf{k}_Q^s) + a_{\text{ref}}^{\mu} + r_1^{\mu\nu}(\mathbf{k}_Q^s - \mathbf{g}) \times a^{\nu}(\mathbf{k}_Q^s - \mathbf{g})\exp(\mathrm{j}g\Delta x). \quad (10)$$

For simplicity, from now on let us assume that both the incident and the reference waves are perfectly planar. This does not change any general outcome. Also, for simplicity of notation, let us drop the wavevector $\mathbf{k}_Q^s$ in $b_{\Delta x}^{\mu\nu}(\mathbf{k}_Q^s)$ from now on. From equation (10), the interference is now a three wave one, and the intensity can be written as

$$\begin{aligned} I_{\beta\Delta x,\alpha}^{\mu\nu} &= |b_{\beta\Delta x}^{\mu\nu} + a_{\text{ref};\alpha}^{\mu}|^2 \\ &= |b_{\beta\Delta x}^{\mu\nu}|^2 + |a_{\text{ref};\alpha}^{\mu}|^2 + 2|b_{\beta\Delta x}^{\mu\nu}||a_{\text{ref};\alpha}^{\mu}| \\ &\quad \times \cos[(\arg b_{\beta\Delta x}^{\mu\nu} - \arg a_{\text{ref};\alpha}^{\mu})], \end{aligned} \quad (11)$$

where $\arg a_{\text{ref};\alpha}^{\mu}$ is the phase of the $\alpha$th phase step of the reference wave polarized along $\mu$, $\alpha = (0, 1, \ldots, \alpha_{\min} - 1)$ and the scan positions are numbered by the indices $\beta = (0, 1, \ldots, \beta_{\min} - 1)$; for each $\beta$ a specific scan position $\beta\Delta x$ is chosen. Since these scan positions are used for providing successive phase shifts usually they are chosen equidistantly. Physically, $I_{\beta\Delta x,\alpha}^{\mu\nu}$ implies, following the notation for scanning and phase steps as introduced before, the intensity for the $\alpha$th phase step measured at the $\beta_m$th scanning position. The complete experimental setup will now result in a modified coherent scatterometry setup [15], shown schematically in figure 3(b).

To understand the minimum number of frames required for one specific polarization scheme, it may be noted from equation (10) that the first and zeroth order complex reflection amplitudes add up to the complex number $b_{\beta\Delta x}^{\mu\nu}$ in equation (8). The latter complex number is derivable from phase-shifting interferometry with a reference wave. However, to solve a system of equations as in equation (8), we need two measurements, i.e. two scan positions ($\beta_{\min} = 2$), since each of them contains two independent complex numbers, namely $r_0^{\mu\nu}(\mathbf{k}_Q^s)$ and $r_1^{\mu\nu}(\mathbf{k}_Q^s - \mathbf{g})$. Thus, the minimum number of frames required for measurement of one specific polarization scheme in ICFS is six, employing three-step phase-shifting interferometry each with two scanning positions ($\alpha_{\min} = 3$, $\beta_{\min} = 2$).

This argument can easily be extended when more orders are overlapping ($F < 1$). For example, if three orders are overlapping, $b_{\beta\Delta x}^{\mu\nu}$ will contain three independent complex numbers, and we will need nine measurements ($\alpha_{\min} = 3$, $\beta_{\min} = 3$). Successive overlapping orders will increase $\beta_{\min}$ by one each. An interesting remark can be made here by noting that ICFS, i.e., CFS with interference with a reference wave, leads to a smaller minimum number of scanning positions than the CFS setup without interferometry with the reference wave.

Together, all the interferometric and scanning frames are considered as one set of intensity data, a scatter-interferometry super-frame. After this super-frame is defined, standard sensitivity analysis for scatterometry [16] of the model with respect to the required shape parameters can be carried out. Assuming a noise independent of pixel location and having a normal distribution with unit standard deviation, the 3-sigma uncertainty per pixel $\Delta a_l$ for the $l$th shape parameter is given by [17]

$$\Delta a_l = 3\sqrt{C_{ll}}, \quad (12)$$

where $\mathbf{C}$ is the covariance matrix of the grating shape parameters for the model. According to the standard practice of optimization, we arrange the shape parameters (figure 3) in one vector $\mathbf{a} = (a_1, a_2, a_3) = (\text{height, swa, midcd})$, and the $l$th component of that vector has uncertainty $\Delta a_l$. Now we can define the coherent sensitivity gain due to interferometry, **csgi**, as

$$\text{csgi}_l = \frac{\Delta a_{l,\text{scatterometry without interferometry}}}{\Delta a_{l,\text{scatterometry with interferometry}}}, \quad (13)$$

where it is assumed that for scatterometry without interferometry sufficient scanning is already carried out to obtain maximum possible sensitivity. It is to be noted that any pixel independent noise component influencing CFS and ICFS in the same way will cancel out in the way **csgi** has been defined, making the results independent of any sensitivity gained or lost due to this noise.

## 3. Results and discussion of sensitivity analysis

In this section, we consider example gratings of different pitches to evaluate the sensitivity gain and to verify the assumptions made through numerical simulations using rigorous coupled wave analysis (RCWA) [18, 19]. The independent variable is the overlap parameter which can be varied from $F = 1$ to some reasonable upper limit such that the case where only the zeroth order is present is also considered. In the following simulations, we set this upper limit as $F = 2.2$. The reason for limiting the scope of this paper to gratings that are not highly sub-wavelength is mainly because a simpler theory can be used to describe them more efficiently [20], which is beyond the present discussion. However, this range will be sufficient to show the effectiveness of the principle discussed. We set the simulation

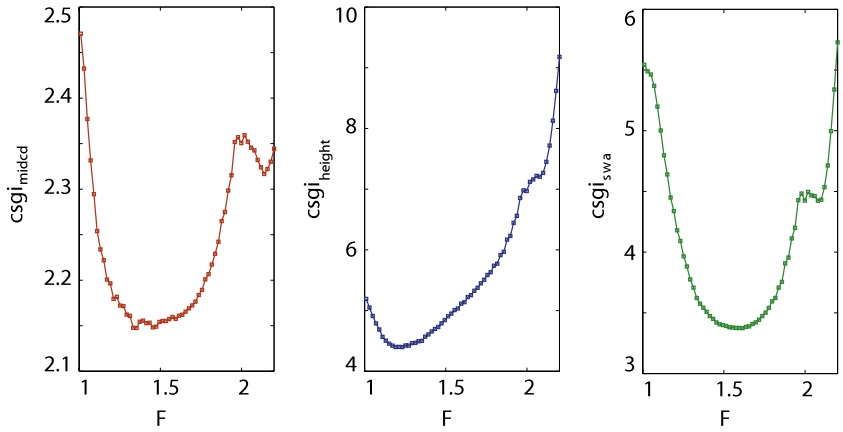


**Figure 4.** Gain in sensitivity of ICFS compared to CFS when **csgi** as a function of overlap parameter $F$ is plotted for midcd (left), height (center) and swa (right) in the range $1.01 \leq F \leq 2.2$. Improvement in sensitivity is seen for all cases.

**Table 1.** The simulation parameters summarized.

| | Simulation settings | | |
|---|---|---|---|
| Grating type | Binary symmetric, resist on silicon in air | | |
| Grating shape | 150 nm (height) | 90° (swa) | 0.5 (duty cycle) |
| Overlap parameter settings | $\lambda = 633$ nm | NA $= 0.9$ | Variable $\Lambda$ |

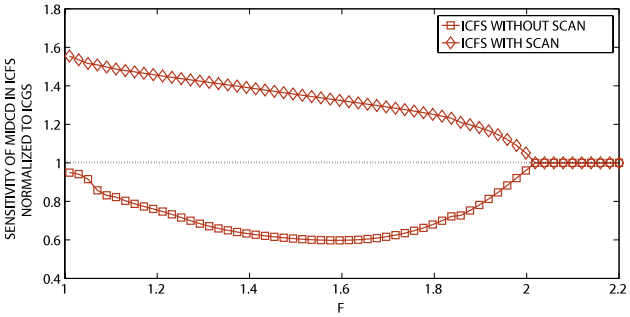


**Figure 5.** The sensitivity of ICFS is compared with ICGS. The sensitivity in ICFS for midcd is normalized with the sensitivity of interferometric coherent goniometric scatterometry and plotted with the overlap parameter for the cases when scanning is carried out (◊) and not carried out (□). The results show that with scanning the sensitivity in ICFS becomes better when $F \leq 2$. When $F > 2$, the sensitivities of both methods are the same.

wavelength at $\lambda = 633$ nm and assume an NA of 0.9, while the pitch is variable. The duty cycle is fixed at 0.5 so that *midcd* scales linearly with the pitch. In table 1, we summarize the simulation parameters.

In figure 4, the results for ICFS are shown. It is seen that **csgi** $> 1$ for *all* values of the overlap parameter and for *all* parameters, proving the benefits of ICFS. Depending on the specific value of the overlap parameter the gain is seen to vary. This indicates that for these given physical variables (wavelength, NA, grating material, etc) some specific grating shapes have more sensitivity than others. Similar conclusions can be drawn from the results observed for gratings with other shapes and materials which have also been tested but left out to avoid repetition.

At this point, it will be interesting to make a comparison of ICFS with coherent goniometric scatterometry. As mentioned in section 1, integration with interferometry can also be performed for this technique, and if we repeat the experiment for each of the incident waves in the NA we can make a fair comparison with ICFS. As the scattered field of each incident plane wave will have to be interfered with the reference beam separately, this process will be very slow and have little practical importance. Nonetheless, the comparison with ICFS will show how important the benefits are of the previously discussed retrieval of overlapping orders by scanning. Since normally (to save time) goniometric scatterometry is performed for planar incidence only [13], a linear array along the $x$-axis ($\eta = 0$) will be considered for the interferometric versions of both methods. This comparison is shown for midcd in figure 5. Here, the sensitivity of ICFS is normalized with the interferometric version of coherent goniometric scatterometry for two cases: no scanning ($\beta_{\min} = 1$) and sufficient scanning[3]. For $F > 2$, we observe that the sensitivities of both methods are identical. To explain this, firstly we note that all calculations for goniometric scatterometry require only $\mathbf{R}_m^R$ mentioned in equation (7). As $F > 2$, only the zeroth order is captured ($f = 1$ in equation (7)), and the sensitivities from both methods should be identical because the rotation matrices in equation (7) cannot add any overall gain in sensitivity. This can be used as a check for correctness in modeling both methods. For $F \leq 2$, without scan, the sensitivity of ICFS is poorer than its goniometric counterpart. However, the situation changes when scanning is performed because then ICFS is seen

[3] As goniometric scatterometry has no superposition, scanning is unnecessary.

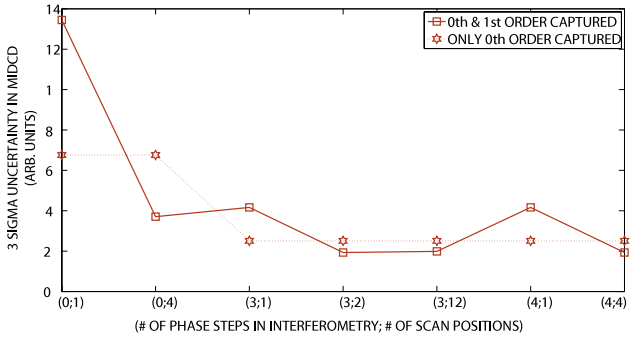


**Figure 6.** Verification of equation (11) is shown for two overlap parameters: $F = 1.59$ (□ —), when the 0th and the 1st orders are present, and $F = 2.08$ (⋆ · · ·), when only the 0th order is present. The abscissa denotes different cases of interference and scanning as ordered pairs, where the first number is the number of phase steps in interferometry and the second is the number of scanning positions. The 'saturation' of sensitivity shows no more sensitivity gain beyond (3; 2) for both gratings, agreeing with the predictions made after equation (11).

to have more sensitivity. This seems surprising at first, as both techniques must have the same physical information. The explanation for this observation can be found from the way in which this information is arranged in the intensity measurements of the two cases. To explain this, we expand equation (11),

$$\begin{aligned} I^{\mu\nu}_{\Delta x,\alpha}(\mathbf{k}^{\mathrm{s}}_{\mathrm{P}}) = {} & |r^{\mu\nu}_0|^2 + |r^{\mu\nu}_1|^2 + 1 + 2|r^{\mu\nu}_0| \\ & \times \cos[(\arg r^{\mu\nu}_0 - \arg a^{\mu}_{\mathrm{ref};\alpha})] + 2|r^{\mu\nu}_1| \\ & \times \cos[(\arg r^{\mu\nu}_1 + g\Delta x - \arg a^{\mu}_{\mathrm{ref};\alpha})] \\ & + 2|r^{\mu\nu}_0||r^{\mu\nu}_1| \\ & \times \cos[(\arg r^{\mu\nu}_0 - \arg r^{\mu\nu}_1 - g\Delta x)], \end{aligned} \tag{14}$$

where we assumed a normalized intensity for the plane reference wave. Here, we have dropped the functional dependence of $r^{\mu\nu}_0$ and $r^{\mu\nu}_1$ on $\mathbf{k}^{\mathrm{s}}_Q$ and $\mathbf{k}^{\mathrm{s}}_Q - \mathbf{g}$, respectively, to make the equation compact assuming they are implied implicitly. If we take the derivative of equation (11) with respect to any shape parameter, the contribution of the last term is only available in ICFS. Independent of the phase of the reference, without scanning, this term can be seen as an additional noise component with unpredictable contribution towards sensitivity, while with scanning, this gives the gain in sensitivity. From the point of view of determination of the scattering matrices of the system, interferometric goniometric scatterometry is simpler, since there is not need to retrieve overlapping orders. However, owing to the overlap, ICFS has superior sensitivity and is *more* suitable for use in an optimization algorithm.

In figure 6 we test the remarks made after equation (11) about the values of $\alpha_{\min}$ and $\beta_{\min}$. We designate our scatter-interferometry super-frame by $(\alpha_{\min}; \beta_{\min})$. For example, (0; 4) will mean scatterometry without interferometry with four independent scanning positions; likewise, (3; 12) implies scatterometry with three-frame phase-shifting interferometry and 12 scanning positions. If we notice the 3-sigma uncertainty in midcd for two specific overlap parameters, then we can see for the specific grating with $F = 1.59$ (overlap between orders) the the minimum is obtained for (3; 2); (3; 12) and (4; 4), whereas for the case $F = 2.08$ (only 0th order), there is no change after (3; 1). Thus it is seen that when there is overlap, $(\alpha_{\min}, \beta_{\min}) = (3; 2)$ is sufficient and for no overlap, $(\alpha_{\min}, \beta_{\min}) = (3; 1)$ is sufficient[4]. If we compare the (0; 4) and (3; 2), we can see that the increase in sensitivity is comparatively larger for $F > 2$, about three times, than for $F \leq 2$, when it is about two times. Finally, we may note that a measurement scheme of (3; 2) for $F > 2$ and (3; 0) for $F \leq 2$ should provide sufficient information to obtain scattering matrices. For this reason, more intensity measurements did not lead to any gain in sensitivity. This remark supports the assumptions made after equation (11).

## 4. Conclusion

In this paper we have shown how coherent Fourier scatterometry can benefit from integration with phase-shifting interferometry to improve the sensitivity. It was pointed out [6] that one of the advantages of CFS compared to other angular scatterometry methods is the fact that a number of plane waves from different directions are incident simultaneously due to the focusing of the objective, creating superposition and consequent enhancements of sensitivity. We showed how the benefits of coherence can be extended even more with integration of scatterometry with interferometry. Moreover, unless the pitch is sufficiently large, overlap between orders does not occur and CFS does not have any practical advantage in terms of sensitivity compared to incoherent Fourier scatterometry. With ICFS, improvement of sensitivity for these cases is also shown. Common practical difficulties (like vibrations, stability of incident wave) associated with interferometric analysis are often taken care of by more phase steps and stabilized instrumentation. These problems are more critical for explicit phase retrieval, which is required if the scattering matrix is to be determined. However, in semiconductor metrology this is not needed. In a comparison with coherent goniometric scatterometry, we showed that even though these two systems contain the same physical information about the sample, with scanning, ICFS shows superior sensitivity. This is desirable for fast convergence of any optimization algorithm, a fact that is important for industrial applications.

## Acknowledgments

The authors acknowledge Mark van Kraaij for the RCWA routine. They also acknowledge Omar El Gawhary and Peter Petrik for their valuable suggestions and comments.

## References

[1] International Technology Roadmap for Semiconductors 2011 www.itrs.net/reports.html
[2] Rice B J, Cao H, Grumski M and Roberts J 2005 *AIP Conf. Proc.* **788** 379

[4] It should be noted that (0; 4) is sufficient for CFS, while (3; 0) is sufficient for interferometric coherent goniometric scatterometry.

[3] American National Institute of Standards and Technology *Optical Grating Scatterometry* www.nist.gov/pml/div685/grp06/scatterometry.cfm
[4] Thony P, Harrison D, Henry D, Severgnini E and Vasconi M 2003 *AIP Conf. Proc.* **683** 381–88
[5] den Boef A J M, Bleeker A J, van Dommenlen Y J L M, Dusa M, Kiers A G M, Luehrmann P F, Pellemans H P M, van der Schaar M, Grouwstra C D and van Kraaij M G G M 2006 *European Patent* EP 1628164
[6] Gawhary O E, Kumar N, Pereira S F, Coene W M J and Urbach H P 2011 *Appl. Phys.* B **105** 775–81
[7] Kumar N, Gawhary O E, Roy S, Pereira S F and Urbach H P private communication
[8] Roy S, Gawhary O E, Kumar N, Pereira S F and Urbach H P 2012 *J. Eur. Opt. Soc. Rap. Public.* **7** 12031
[9] Malacara D, Servin M and Malacara Z 2005 *Interferogram Analysis for Optical Testing* 2nd edn (Boca Raton, FL: CRC Press) chapter 7
[10] Paz V F, Peterhansel S, Frenner K and Osten W 2012 *Light: Sci. Appl.* **1** e36
[11] Rumpf R C 2011 *Prog. Electromag. Res.* B **35** 241–61
[12] Bykov D A and Doskolovich L L 2013 *J. Lightwave Technol.* **31** 793–801
[13] Wurm M, Pilarski F and Bodermann B 2012 *Rev. Sci. Instrum.* **81** 023701
[14] Wurm M, Bonifer S, Bodermann B and Gerhard M 2011 *J. Eur. Opt. Soc. Rap. Public.* **6** 11015s
[15] Kumar N, Gawhary O E, Roy S, Kutchoukov V G, Pereira S F, Coene W and Urbach H P *Proc. SPIE* **8324** 83240Q
[16] Silver R, Germer T, Attota R, Barnes B M, Bunday B, Allgair J, Marx E and Jun J 2007 *Proc. SPIE* **6518** 65180U
[17] Press W H, Flannery B P, Teukolsky S A and Vetterling W T 1995 *Numerical Recipes in C: The Art of Scientific Computing* (Cambridge: Cambridge University Press) pp 657–74
[18] van Kraaij M G M M and Maubach J M L 2004 *Proc. to Progress in Industrial Mathematics at ECMI (Eindhoven)* (Berlin: Springer) pp 164–8
[19] Moharam M G, Pommet D A and Grann E B 1995 *J. Opt. Soc. Am.* **12** 5
[20] Lalanne P and Hugonin J 1998 *J. Opt. Soc. Am.* **15** 7